Organic coating on sulfate and soot particles in summer Arctic atmosphere

Hua Yu[1,2], Weijun Li[2*], Yangmei Zhang[3], Peter Tunved[4], Manuel Dall'Osto[5], Xiaojing Shen[3], Junying Sun[3], Xiaoye Zhang[3], Jianchao Zhang[6], Zongbo Shi[7,8*]

[1]College of Life and Environmental Sciences, Hangzhou Normal University, 310036, Hangzhou, China

[2]Department of Atmospheric Sciences, School of Earth Sciences, Zhejiang University, 310027, Hangzhou, China

[3]Key Laboratory of Atmospheric Chemistry, Chinese Academy of Meteorological Sciences, Beijing, China

[4]Department of Environmental Science and Analytical Chemistry, Stockholm University, 10691, Stockholm, Sweden

[5]Institute of Marine Sciences, ICM-CSIC, Passeig Marítim de la Barceloneta, 37-49, E-08003, Barcelona, Spain

[6]Key Laboratory of the Earth's Deep Interior, Institute of Geology and Geophysics, Chinese Academy of Sciences, 100029, China

[7]School of Geography, Earth and Environmental Sciences, University of Birmingham, Birmingham, UK

[8]Institute of Surface Earth System Science, Tianjin University, Tianjin, China

[*]Corresponding Emails: liweijun@zju.edu.cn; z.shi@bham.ac.uk

Abstract

Interaction of anthropogenic particles with radiation and clouds plays an important role on Arctic climate change. Mixing state of aerosols is a key parameter to influence aerosol-cloud and aerosol-radiation interaction. However, little is known on this parameter in the Arctic, preventing an accurate representation of this information in global models. Here we used transmission electron microscopy with energy-dispersive X-ray spectrometry (TEM/EDS), scanning TEM, scanning electron microscopy (SEM), nanoscale secondary ion mass spectrometry (NanoSIMS), and atomic forces microscopy (AFM) to determine the size and mixing properties of individual particles at 100 nm – 10 μm, with a particular focus on sulfate and carbonaceous particles. We found that non-sea salt sulfate particles with size range at 100-2000 nm were commonly coated with organic matter (OM) in summer. 20% of sulfate particles also had soot inclusions which only appeared in the OM coating. The OM coating is estimated to contribute to 63% of the particle volume on average. To understand how OM coating influences optical properties of sulfate particles, the Mie theory of the core-shell model was applied to calculate optical properties of individual sulfate particles. The result shows that absorption cross section (ACS) of individual OM-coated particles significantly increased when assuming the OM coating as light-absorbing brown carbon (BrC) and the ACS also increased following the increasing particle size. The microscopic observations suggest that OM modulates the mixing structure of fine Arctic sulfate particles, which may determine their hygroscopicity and optical properties.

1. Introduction

Surface temperatures are rising faster in the Arctic than the rest of globe (IPCC, 2013). Although increased human-induced emissions of long-lived greenhouse gases are certainly one of the driving factors, air pollutants, such as aerosols and ozone, are also important contributors to climate change in the Arctic (Law and Stohl, 2007; Shindell, 2007). It is well known that aerosols from northern mid-altitude continents affect the sea ice albedo by altering the heat balance of the atmosphere and surface (Hansen and Nazarenko, 2004; Jacob et al., 2010; Shindell, 2007). These aerosols in Arctic atmosphere include sea salt, sulfate, particulate organic matter (OM), and to a lesser extent, ammonium, nitrate, black carbon (BC) (Hara et al., 2003; Quinn et al., 2007) and mineral dust particles (Dagsson-Waldhauserova et al., 2013). Studies show BC in the Arctic absorbs solar radiation in the atmosphere and when deposited on snow (Iziomon et al., 2006; Koch and Hansen, 2005; Sand et al., 2013; Shindell, 2007). Moreover, Maahn et al. (2017) used aircraft in situ observation of clouds and aerosols and found that concentration of BC are enhanced below the clouds in the Arctic and further influence the mean effective radii of cloud droplets which lead to the suppressed drizzle production and precipitation.

BC, commonly called ‘‘soot’’ is derived from the combustion sources such as diesel engines, residential solid fuel, and open burning (Bond et al., 2013). Some studies investigated the possible sources of these BC particles, including natural gas flaring (Qi et al., 2017) and ship emissions in the Arctic (Browse et al., 2013; Weinbruch et al., 2012) and emissions of biomass burning and fossil fuels in the northern hemisphere (Winiger et al., 2016; Xu et al., 2017). For example, Winiger et al.(2017) showed that most Arctic BC is sourced from domestic activities (35%) and transportation (38%), with only minor contributions from gas flaring (6%), power plants (9%), and open fires (12%).

Accumulation of secondary organic aerosols, a significant fraction of the new particles grows to sizes that are active in cloud droplet formation in the Arctic (Abbatt et al., 2019). More than 100 organic species have been detected in the Arctic aerosols and polyacids are the most abundant compound class, followed by phthalates,

aromatic acids, fatty acids, fatty alcohols, sugars/sugar alcohols, and n-alkanes (Fu et al., 2008). Recently, certain organic aerosols, referred to as brown carbon (BrC), have been recognized as an important light-absorbing carbonaceous aerosol after BC in the troposphere (Alexander et al., 2008; Andreae and Gelencser, 2006; Feng et al., 2013; Lack et al., 2012). BrC can be directly emitted from combustion sources or formed in the atmosphere via photo-chemical aging (Jiang et al., 2019; Saleh et al., 2013; Updyke et al., 2012). Moreover, aging of secondary organic aerosols can significantly contribute to BrC during atmospheric transports (Laskin et al., 2015). Feng et al.(2013) estimated that on average, BrC accounts for 66% of total OM mass globally and its light absorption is about 26% of BC.

BC and BrC are often internally mixed with other non-absorbing aerosols, such as sulfate (Lack et al., 2012; Laskin et al., 2015). Internal mixing means that a single particle simultaneously contains two or more types of aerosol components (Li et al., 2016). This internal mixing can enhance BC absorption by a factor of up to two (Bond et al., 2013) and change the activity of cloud condensation nuclei (CCN) in the Arctic atmosphere (Leck and Svensson, 2015; Martin et al., 2011). Spatial and temporal variations of aerosol composition, size distribution, and sources of Arctic aerosols have been studied extensively in numerous ground-based, ship, airborne observations, and various atmospheric models (Brock et al., 2011; Burkart et al., 2017; Chang et al., 2011; Dall'Osto et al., 2017; Fu et al., 2008; Hara et al., 2003; Hegg et al., 2010; Iziomon et al., 2006; Karl et al., 2013; Lathem et al., 2013; Leck and Bigg, 2008; Leck and Svensson, 2015; Moore et al., 2011; Raatikainen et al., 2015; Wöhrnschimmel et al., 2013; Winiger et al., 2017; Yang et al., 2018; Zangrando et al., 2013). A few previous studies also looked at the mixing states of coarse aerosol particles in Arctic troposphere (Behrenfeldt et al., 2008; Chi et al., 2015; Geng et al., 2010; Hara et al., 2003; Leck and Svensson, 2015; Moroni et al., 2017; Raatikainen et al., 2015; Sierau et al., 2014), but those of fine non-sea salt particles, including the most important short-lived climate forcers – BC and BrC (Feng et al., 2013; Fu et al., 2008; Kirpes et al., 2018; Laskin et al., 2015; Leck and Svensson, 2015), are poorly characterized. The poor understanding on mixing state of BC and BrC in individual

particles will prevent the further simulation of atmospheric climate and aerosol-cloud interaction in the Arctic through the current atmospheric models (Browse et al., 2013; Samset et al., 2014; Zanatta et al., 2018).

In this study, individual aerosol particles were collected in the Arctic during 7-23 August, 2012. We combined the data from various microscopic instruments to systematically determine the size, composition, and mixing properties of individual particles, with a particular focus on sulfate and carbonaceous particles. Mie theory was used to test how OM coating influences optical properties of sulfate particles in the Arctic when OM was assumed as BrC. The results are discussed in the context of aerosol-radiation and cloud interaction.

2. Experimental section

2.1 Field campaign

The Svalbard archipelago includes all landmasses between 74 and 81 degrees North and 10 and 35 degrees East (Figure 1). The islands cover 63000 km^2. Ny-Ålesund town is situated on the west coast of the largest island, Spitsbergen. Ny-Ålesund town is situated only 1200 km from the North Pole and represents a central platform for Arctic research. The sampling place represents remote Arctic conditions.

An individual particle sampler at Chinese Arctic Yellow River Station (78°55′N, 11°56′E) collected individual particles (Chi et al., 2015; Geng et al., 2010). The sampling site is about 2 km far away from the Zeppelin observatory station (78.9N 11.88E) running by the Ny-Ålesund Science Managers Committee (https://www.esrl.noaa.gov/psd/iasoa/stations/nyalesund). Two to three samples were regularly collected at 9:00, 16:00, 21:00 (local time) of each day, with a total of 46 samples during 7-23 August, 2012.

A sampler containing a single-stage impactor with a 0.5-mm-diameter jet nozzle (Genstar Electronic Technology, China) was used to collect individual particles by the air flow rate at 1.5 l min^{-1}. Aerosol particles were collected onto copper TEM grids coated with carbon film. This sampler has a collection efficiency of 31% at 100 nm

aerodynamic diameter and 50% at 200 nm if the density of the particles is 2 g cm^{-3}. The sampler can collect particles with < 10 μm aerodynamic diameter on TEM grids. Sampling times varied from twenty minutes to two hours in clean remote Arctic area. After collection, each sample was placed in a sealed dry plastic tube and stored in a desiccator at 20 ± 3% RH for analysis. Ambient laboratory conditions (17−23% RH and 19−21 °C) is effective at preserving individual hygroscopic aerosol particles and reducing changes that would alter samples and subsequent data interpretation (Laskina et al., 2015). The sample information such as local sampling date and time and meteorological conditions (e.g., temperature (T), relative humidity (RH), pressure (P), wind direction (WD), wind speed (WS)) are listed in Table S1.

2.2 TEM measurement

Individual particle samples were examined by a JEOL JEM-2100 transmission electron microscopy operated at 200 kV with an energy-dispersive X-ray spectrometry (TEM/EDS). TEM can observe the mixing structure of different aerosol components within an individual particle on the substrate because electron beam transmit through the specimen to form an image. EDS spectra were acquired for a maximum time of 30 s to minimize potential beam damage and collect particle X-ray spectra with sufficient intensity. TEM grids are made of copper (Cu) and covered by a carbon-reinforced substrate, so Cu is excluded from the quantitative analyses of the particles. Because of the substrate contribution, C content in TEM grid coated by carbon film might be overestimated in EDS spectra of individual particles.

The distribution of aerosol particles on TEM grids was not uniform, with coarser particles occurring near the center and finer particles on the periphery. Therefore, to ensure that the analyzed particles are representative, five areas were chosen from the center and periphery of the sampling spot on each grid. Through a labor-intensive operation, 2002 aerosol particles with diameter < 10 μm in 21 samples were analyzed by TEM/EDS (Table S1). To check elemental composition of individual particles, EDX was manually used to obtain EDS spectra of individual particles. In the clean Arctic air, there are simply particle types including sea salt, sulfate, soot, and OM.

Because soot particles have chain-like aggregation, it is not necessary to check their elemental composition. Sea salt particles display spherical or square shapes and are stable under the electron beam in TEM but sulfate particles are spherical but flats on the substrate and produce unstable bubble under the electron beam (Buseck and Posfai, 1999; Chi et al., 2015). TEM observations also can clearly identify sulfate particles or sulfate with OM coating. Therefore, we can easily identify Arctic particle types based on their morphology. Because of the time-consuming in the experiment, it is not necessary to frequently check elemental composition of the same particle type. For the data statistic in this study, we randomly checked elemental composition of 20-30 particles in each sample (Table S1). EDS spectra of 575 particles were manually selected and saved in the computer for elemental composition analysis. Particles examined by TEM were dry at the time of observation in the vacuum of the electron microscope. In our study, the effects of water and other semi-volatile organics were not considered as they evaporate in the vacuum.

Elemental mapping and line profile of individual aerosol particles were obtained from the EDX scanning operation mode of TEM (STEM). The STEM information can clearly display elemental distribution in the targeted individual particles which cannot be provided by the above EDS examination. Based on preliminary individual analysis, we further chose the typical samples containing abundant sulfate with OM coating for the STEM analysis. The high-resolution details of elemental distribution in individual particles can further prove the details of the mixing structure of sulfate and OM in individual particles.

The iTEM software (Olympus soft imaging solutions GmbH, Germany) is an image analysis platform for electron microscopy. In this study, it was used to manually or automatically obtain area, perimeter, and equivalent circle diameter (ECD) of individual particles through identifying boundary of every particle in TEM images. In these analyzed samples, we found there were abundant fine sulfate particles in 11 samples collected during 9-15 August, 2012. In other samples, there were only a few sulfate particles and more sea salt particles. Based on the TEM observations, we selected the samples containing more sulfate particles to further do

other microscopic analyses as below.

2.3 NanoSIMS measurement

Because the sulfate particles collected in the Arctic had good consistent property (e.g., elemental composition and mixing state) from TEM observations, we just selected three samples containing abundant fine sulfate particles (Table S1) for further studies. These three samples listed in Table S1 were analyzed using a nanoscale secondary ion mass spectrometry (NanoSIMS) 50L (CAMECA Instruments, Geneviers, France) instrument. A micro-cesium source was used to generate Cs^+ primary ions, with an impact energy of 16 kV for sample interrogation. The primary beam was stepped across the sample to produce element specific, quantitative digital images. The Cs^+ primary ion beam was used to obtain $^{16}O^-$, $^{12}C^{14}N^-$, $^{14}N^{16}O^-$, $^{32}S^-$, $^{35}Cl^-$, and $^{16}O^{23}Na^-$ ions in this study. The NanoSIMS analysis can obtain ion mapping of particles with nanometer spatial resolution over a broad range of particle sizes (Figure S1). Because the substrate of TEM grid is carbon, CN^- is adopted to represent OM in individual particles (Chi et al., 2015; Ghosal et al., 2014). S^- is used to infer the presence of sulfates in individual particles (Li et al., 2017). Finally, the NanoSIMS obtained ion mapping of 32 sulfate particles.

2.4 SEM and AFM measurement

Because TEM could not vertically observe OM coating and sulfate core, we conducted one special experiment using a Zeiss ultra 55 scanning electron microscopy (SEM) with EDS. The TEM grids were mounted onto an aluminum SEM stub and directly observed in secondary electron image mode. SEM analysis was operated at 10 kv of extra high tension (EHT) and 9.7 mm of work distance (WD). Processes such as sample moving, analysis region selection and imaging were controlled by computer. The specimen stage in SEM was tilted at the range of 0-75^o, and then we vertically observed thickness of OM coating and sulfate core on the substrate. To verify vertical property of individual S-rich particles impacting on the substrate, we observed two typical samples containing abundant sulfate particles using the SEM (Table S1).

AFM with a digital nanoscope IIIa instrument operating in the tapping mode was used to observe surface morphology of individual aerosol particles and measure particle thickness. The tapping AFM has a cantilever and conical tip of 10 nm radius. By using AFM, a general image of the particles is taken at 10 μm full scan size, which generally includes 1-2 particles depending on the exact location. In this study, we are only interested in the sulfate-containing particles. AFM provides surface information and morphology of 17 particles but no composition. Samples were firstly quickly examined by the TEM under low magnification mode. In case, the operation roughly identified S-containing particles and didn't damage the secondary sulfate particles under the electron. Because TEM grids have coordinates letters, we can exactly find the same particles on the substrate in AFM examined in TEM experiments. The procedures can exclude sea salt particles in the AFM image. As a result, the same samples observed by TEM were then examined in AFM to obtain 3-D image of secondary sulfate particles and their volume. Because individual particles collected in Arctic air were scattered on the substrate, we only obtained 17 effective data. After we obtained AFM images of sulfate particles, the NanoScope analysis software can automatically obtain bearing area (A) and bearing volume (V) of each analyzed particle according to the following formula.

$$A = \frac{4}{3}\pi r^2 = \frac{\pi d^2}{3} \rightarrow d = \sqrt{\frac{3A}{\pi}} \quad (1)$$

$$V = \frac{4}{3}\pi r^3 = \frac{4}{3} \times \frac{\pi D^3}{8} \rightarrow D = \sqrt[3]{\frac{6V}{\pi}} \quad (2)$$

Where x is the equivalent circle diameter (ECD) and y is the equivalent spherical diameter (ESD).

ECD of individual aerosol particles measured from the iTEM software can be further converted into ESD. Based on these data, we estimate one good linear correlation (y=0.38x) between ESD and ECD of sulfate particles impacting on the substrate. The value was further used to correct all the analyzed particles in TEM images (Chi et al., 2015).

2.5 Calculation of BrC optical properties

The refractive index used for the non-light-absorbing sulfate component was set to m=1.55 at 550 nm (Seinfeld and Pandis, 2006). The refractive index of OM (as BrC) is not known so we considered three scenarios: strongly absorbing (1.65-0.03i at 550 nm), moderately absorbing (1.65-0.003i at 550 nm), and non-absorbing OM (1.65 at 550 nm) (Feng et al., 2013). Although the refractive index has dependence on the wavelength between 350-870 nm, we tried to select the 550 nm as a case to test how OM coating influence sulfate particles in Arctic air.

BHCOAT Mie code by Bohren and Huffman (1983) was used to calculate the optical properties, including scattering cross section (SCS), absorption cross section (ACS), and single scattering albedo (SSA), assuming a core-shell structure. We firstly calculated these parameters assuming a sulfate core and OM shell structure only (ignoring some of the particles that contain soot core). Because the Mie code only can calculate the core-shell structure or homogeneous models, we assume sulfate as a core and OM as a shell in individual particle to build the core-shell model. Based on the core-shell standard mode (Li et al., 2016), we can calculate optical properties of individual internally mixed particles.

2.6 Back trajectories of air masses and Lagrangian particle dispersion model

Three-day (72 h) back trajectories of air masses were generated using a Hybrid Single Particle Lagrangian Integrated Trajectory (HYSPLIT) model at the Chinese Arctic Yellow River Station during August 2012, at an altitude of 500m above sea level (Figure 1). Most air masses originate in the Arctic Ocean, and are restricted to this vast marine region during the sampling periods. Based on the TEM observations, air masses from North America and Greenland brought abundant sulfate particles into the sampling area in summertime.

In order to determine the particle origins, the lagrangian particle dispersion model FLEXPART-WRF 3.1 (Brioude et al., 2013) was used. The FLEXPART-WRF model is using meteorological parameters from WRF dynamical simulation. The domain resolution is 50×50 km with 64 vertical levels. The FLEXPART-WRF simulations were launched in a backward mode over 10 days, with the Chinese Arctic Yellow

River Station as an origin. For each simulation (one per sample), 20000 pseudo-particles were released in a small volume around the station position. Each single particle position evolution backward in time was determined by Lagrangian dispersion calculation. Based on the TEM experiments and back trajectory of air masses (Figure 1), we found that there were more S-rich with OM coating particles in the samples collected on August 11, 12, 14 and 15, 2012. Therefore, we further did the FLEXPART-WRF simulation of these four days (Figure 2). The emission intensity in the Arctic area has been also shown in Figure S2.

3. Results

3.1 Composition and sources of aerosol particles

We summarized average elemental weight and frequency of individual Arctic particles derived from the TEM/EDX. The result shows that O, Na, S, and Cl in individual particles are dominant elements (Figure S3). On basis of the composition and morphology of individual particles, we classified the particles into four major groups: Na-rich (i.e. NaCl, Na_2SO_4, and $NaNO_3$), S-rich (i.e. ammonium sulfate and sulfuric acid), and carbonaceous (soot and OM). The classification criteria of different particle types and their sources have been described in a separate study (Li et al., 2016). S-rich particles representing secondary inorganic particles (e.g., SO_4^{2-}, NO_3^-, and NH_4^+) are transformed from gaseous SO_2, NO_x, and NH_3. OM can be divided into primary organic matter (POM) and secondary organic matter (SOM). SOM is produced from the chemical oxidation of volatile organic compounds (VOCs) and often exhibits OM coating on S-rich particles. Na-rich particles in the marine air are from sea spray and have typical near cubic shape. Soot particles, which contain C with minor O, appear as a chain-like aggregate of carbon-bearing spheres. Our previous study well characterized aging mechanism of sea salt particles in summer Arctic air (Chi et al., 2015). Here we focused on S-rich, soot, and OM particles as the major non-sea salt particle (NSS-particle, 39±5%) in the analyzed samples, which are approximately 29±7% of 2002 particles (Figure 3).

3.2 OM coating on sulfate particles

TEM observations revealed a common core-shell mixing structure in fine sulfate particles (Figure 4a). Elemental mapping of such internally mixed sulfate particles shows C signals in the coating (C map, Figure 4b) and S and O signals in the center (S and O map, Figure 4c, d). The elemental line profile of a sulfate particle also shows sulfate core and C coating (Figure S4). Furthermore, ion maps of individual particles from the NanoSIMS further exhibite $^{12}C^{14}N^-$ signals in the coating (red color in Figure 4e, f) and $^{32}S^-$ signals in the core (green color in Figure 4e, g). These results provide strong evidence that the coating is OM and the core is sulfate.

A majority of 781 analyzed NSS-particles (74% by particle number) have a sulfate core and OM coating (Figures 4 and 5). ~20% of them also contain small soot inclusions but they only appeared in organic coating, rather than as the core mixed in sulfate (Figure 5b). The mixing structure is different from our previous findings in polluted air that soot is normally mixed with sulfate instead of OM coating (Li et al., 2016). Moreover, we noticed that a few chain-like soot aggregates (1.3% in all analyzed particles) (Figure S5) only occurred in three samples during the sampling period (Table S1). Considering the remoteness of the sampling site, such fresh soot particles are likely to be of local origin, including shipping and flaring (Gilgen et al., 2018; Peters et al., 2011). Indeed, we found a few of ships moving in Arctic Ocean during these days from the Ny-Ålesund town.

TEM observations showed that some sulfate particles had unique morphology that a sulfate particle was surrounded by some smaller particles (Figure 5a). They are often called “satellite” particles as they were distributed from the central particles when impacted on the substrate during sample collection. 16% of the analyzed sulfate particles with satellite particles as shown in Figure 5a were detected in the samples (Table S1) collected during 9-15 August. NanoSIMS analysis further provided more information that the satellite particles selected from the samples (Table S1) have strong $^{32}S^-$ (Figure 6a, c) and $^{16}O^-$ signals (Figure 6d) as well as weak $^{12}C^{14}N^-$ signals (Figure 6a, b). The CN^- signal normally can represent organic aerosols (Chi et al., 2015; Ghosal et al., 2014). Previous studies showed that the similar satellite particles are normally considered as acidic sulfate (Buseck and Posfai, 1999; Iwasaka et al.,

1983). Therefore, we can conclude that these acidic satellites not only contain sulfuric acid but also some OM or organic acids. Indeed, Fu et al. (2008) found that polyacids are the most abundant organic compounds, followed by phthalates, aromatic acids, and fatty acids in Arctic aerosol particles. As a result, these Arctic sulfate particles with satellites contain certain amounts of sulfuric or organic acids with liquid phase. Back trajectories of air masses and FLEXPART both shows abundant sulfate particles and some containing satellite particles were transported from Greenland and North American (Figures 1 and 2).

AFM was used to obtain 3D image of individual secondary particles impacting on the substrate. Figure 7a shows that the secondary particles normally have smooth surface which is different from uneven surface of the Arctic fresh and aged NaCl particles (Chi et al., 2015). Furthermore, we observed particle thickness through tilting the specimen stage up to 75^{o} in SEM. Figure 7a-b both shows that the secondary particles look like thin pancake sticking on the substrate. Furthermore, the sections of two secondary particles in the AFM images shows that the highest heights of particles are only 0.15 (green line) and 0.26 (red line) of the corresponding horizontal size (Figure 7a). Here we can conclude that shape of individual particles was modified when they impacted on the substrate following the airflow. Therefore, the measured ECDs of individual particles in TEM images are much larger than the real particle diameter. To calibrate the particle diameter, we obtained volume of dry particles on the substrate and then calculated their equivalent sphere diameter (ESD) in the AFM images (Figure 7c). ESD distribution of the secondary Arctic particles displayed a peak at 340 nm, ranging from 100 nm to 2000 nm (Figure 7d). The core particles, as sulfate or soot, had a peak at 240 nm and 120 nm, respectively (Figure 7d). In the core-shell particles, we knew size in all the analyzed particles and further calculated volume of sulfate, OM, and/or soot within individual particles. We can estimate that OM on average accounted for 63±23% of the dry sulfate particle volume. Our result shows that the OM volume increases following the particle size increase (Figure S6).

4. Discussion

4.1 Mixing mechanism of organic, soot, and sulfate

Lagrangian particle dispersion modeling using the FLEXPART-WRF 3.1 showed that air masses arriving at the sampling site during our field measurement periods were likely originated from the Greenland and North America (Figure 2). Previous studies reported that air masses from North America or Greenland during the summer contain higher concentration of black carbon, OM, and sulfate (Burkart et al., 2017; Chang et al., 2011; Fu et al., 2008; Moore et al., 2011; Park et al., 2013). Indeed, there is strong emission intensity of OC and SO_2 around the Arctic area from emission simulation as shown in Figure S2. However, Weinbruch et al. (2012) observed soot particles when cruise ships were present in the area around Ny-Ålesund town. It is possible that minor soot particles are sourced from the ship emissions and most of them are transported from out of Arctic area in the free troposphere (Figure S2).

The sulfate core-OM shell structure observed in the Arctic summer atmosphere is similar to those in the background or rural air in other places (Li et al., 2016; Moffet et al., 2013). Based on the images from electron microscopies, we can infer that OM coating thickness in the Arctic air was comparable with them in rural places but higher than them in urban places. During the transports, organic coatings on sulfates were considered as the secondary organic aerosols and their masses increase following particle aging and growth (Li et al., 2016; Moffet et al., 2013; Sierau et al., 2014). Figures 1 and 2 show that most of particles in the air masses transported long distance from North American. The result indicates that these long-range transportation of secondary sulfate particles have enough time to experience the possible atmospheric heterogeneous reactions on particle surfaces or cloud processes in the Arctic air. Similarly, Moffet et al. (2013) found that soot inclusions occurred in OM coating when OM coating on sulfates built up through photochemical activity and pollution buildup the Sacramento urban plume aged. On the other hand, the sulfate/OM particles with soot inclusions are probably formed in a similar way as those found elsewhere (Li et al., 2016) – e.g., soot particles may have acted as nuclei for secondary sulfate or organic uptake during their transports (Riemer et al., 2009).

Similarly, besides the OM coating in the Arctic particles, Leck and Svensson (2015) found some biogenic aerosols like gel-aggregate containing bacterium in ultrafine particles. However, we didn't find any gel-like particles in the samples because our sampler had very low efficiency for ultrafine particles.

TEM images show that most of the internally mixed sulfate particles display sulfate core and OM coating on the substrate (Figures 4a and 5b, c). The sulfate and OM separation in individual particles were defined by You et al. (2012) as liquid-liquid phase separation (LLPS). Concerning the knowledges of the LLPS can better understand particle hygroscopicity, heterogeneous reactions of reactive gases on particle surface, and organic aging (You et al., 2012). They also reported that the LLPS can reflect the O:C ratio in the OM, which is roughly ≤ 0.5. In this study, we did observe the LLPS in almost all the fine sulfate particles, which indicates that the secondary OM in the coating might be not highly aged. Therefore, we speculate that the thick OM coatings were consistently built up during the long-range transport of sulfate particles and part of secondary OM in the coating likely formed in Arctic area. Indeed, some studies reported that there are various sources of organic precursors during the Arctic area, such as biogenic VOCs from ice melting and open water (Dall'Osto et al., 2017) and anthropogenic VOCs from shipping emissions in summertime (Gilgen et al., 2018). The dependence of OM volume on particle size (Figure S6) suggests that the suspended sulfate particles are initially important surface for secondary OM formation. Moreover, the common OM coating on sulfate particles indicates that secondary OM as the surfaces of fine particles might govern the possible heterogeneous reactions between reactive gases and sulfate particles in the Arctic air.

It should be noted that most of secondary OM not only occurred on the surfaces of sulfate particles but also its mass (mean mass at 63±23%) dominated in individual particles (Figure 7d). The OM dominating in individual particles can influence the IN and CCN activities of secondary sulfate particles (Lathem et al., 2013; Martin et al., 2011). For example, some studies found that an increase in organic mass fraction in particles of a certain size would lead to a suppression of the Arctic CCN activity

(Leck and Svensson, 2015; Martin et al., 2011). Moreover, OM as particle surfaces can significantly influence hygroscopicity and IN activity of sulfate particles (Wang et al., 2012).

4.2 Potential impact of OM on optical properties of sulfate-containing particles

The internal mixing of soot, sulfate, and OM can change optical properties of individual particles in the atmosphere. Recent studies showed that BrC has been detected in the OM in the polluted and clean air and even in upper troposphere (Laskin et al., 2015; Wang et al., 2018). Feng et al. (2013) further calculated the contribution up to 19% of the optical absorption of the strongly absorbing BrC in global simulations which is after the absorption BC aerosols. Although we didn't directly measure the optical absorption and BrC in the Arctic atmosphere, various colored OM (e.g. nitrated/polycyclic aromatics and phenols), referred as BrC, were detected in the Arctic atmosphere in different seasons (Fu et al., 2008; Wöhrnschimmel et al., 2013; Zangrando et al., 2013) and in surface ice or snowpack (Browse et al., 2013; Doherty et al., 2013; Hegg et al., 2010). We also noticed that the $^{12}C^{14}N^-$ signal generally occurred in all analyzed OM coating in sulfate particles (Figure 4e-f). Herrmann et al. (2007) considered that $^{12}C^{14}N^-$ from NanoSIMS represents nitrogen-containing organic in the detected materials. In this study, although we could not determine that all the organic materials in the OM coating were nitrogen-containing OM, the NanoSIMS data as shown in Figure 4 indicated that the OM coating more or less homogenously contained nitrogen-containing OM. As a result, the nitrogen-containing OM indicates that the OM coating could contain certain amounts of secondary BrC (Jiang et al., 2019; Laskin et al., 2015).

To understand how OM coating influence optical properties of sulfate particles, we assume three scenarios of OM coating as BrC: strongly absorbing (case 1), moderately absorbing (case 2) or non-absorbing OM (case 3) with a refractive index of 1.65-0.03i, 1.65-0.003i, and 1.65 at 550 nm according to *Feng et al.* (2013). Based on the size measurements shown in Figure 7d, we can calculate volume of sulfate and OM within each particle. We input volume of each component and the corresponding

refractive index into the Mie code and then calculated optical properties of individual sulfate particles in the samples. Based on optical data statistic of 575 particles, Figure 8a show that the OM coating is strongly absorbing BrC (referred to case Abs1), as by Feng et al.(2013), the average absorption cross section (ACS) of individual particles is estimated to be 2.67×10^{-14} m^2. This value is 8.30 times higher than the aerosol ACS (3.22×10^{-15} m^2) when assuming that the BrC is moderately absorbing (referred to case Abs2, Figure 8a). However, the scattering cross section (SCS) of individual particles only shows a small change (Figure 8b). Figure 8c also shows that the single scattering albedos (SSAs) of individual particles are 0.92, 0.99, and 1 when assuming the BrC as strongly, moderately and non-absorbing (cases SSA1 to SSA3). These results suggest whether we consider organic coating as BrC may have a significant influence on the absorption properties of individual sulfate particles.

In this study, we expored the relationship between ACS of individual particles and particle diameters. Interestingly, Figure 8d shows that ACS of individual fine OM-coating sulfate particles increased following the increasing particle size. The result shows that the ACS can be enhanced following particle size growing and particle aging. In other word, OM-coating sulfate particles transported more longer distances and they might have stronger optical absorption in the Arctic air.

Current climate models estimated the radiative force of Arctic BC (Sand et al., 2013; Shindell, 2007; Winiger et al., 2017; Zanatta et al., 2018), but none specifically considered optical properties of Arctic BrC. Our study well revealed OM coating on sulfate particles and this detail microphysical complexity of aerosol particles will be useful to construct the atmospheric radiation and CCN/IN simulation in Arctic atmospheric models in the future.

5 Summary

Different individual particle techniques, such as TEM/EDS, STEM, SEM, NanoSIMS, and AFM, were applied to study S-rich, soot, and OM particles in the Arctic air in summer. Sulfate particles accounted for approximately 29±7% by number of all analyzed particles in Arctic air. TEM and NanoSIMS commonly

observed OM coating and sulfate core individual sulfate particles, defined as the LLSP. The common OM coating on sulfate particles indicates that secondary OM as the surfaces of fine particles might govern the possible heterogeneous reactions between reactive gases and sulfate particles in the Arctic air. Moreover, 20% of them also contain small soot inclusions but they only appeared in organic coating, rather than as the core mixed in sulfate. The mixing structure is totally different from the previous findings that soot is internally mixed with sulfate instead of OM coating in urban polluted air.

Size distribution of the secondary Arctic particles displayed a peak at 340 nm, ranging from 100 nm to 2000 nm. The core particles, as sulfate or soot, had a peak at 240 nm and 120 nm, respectively. Furthermore, we can estimate that OM on average accounted for 63±23% of the dry NSS-particle volume. Based on microscopic measurements of individual particles, we not only built up one core-shell model but also quantify volume of OM and sulfate in individual particles. The Mie code was used to calculate optical properties of internally mixed sulfate/OM particles when we considered OM as non-absorbing, moderately absorbing BrC, and strongly absorbing BrC. We found that the aerosol ACS is 8.30 times higher than the BrC as moderately absorbing. We concluded that whether we consider organic coating as BrC may have a significant influence on the absorption properties of individual particles in the Arctic air. Moreover, individual fine OM-coating sulfate particles increased following the increasing particle size. Therefore, we proposed that further studies should focus on the BrC in Arctic aerosols: What mass concentrations of BrC are in fine particles? What kinds of BrC are in fine particles? The optical mass absorption of BrC in fine particles should be investigated? These results can be used to evaluate how BrC aerosols influence the Arctic climate.

Author Contributions: WL and ZS designed the study. YZ and XS collected aerosol particles. WL, HY, and JZ contributed laboratory experiments and data analysis. HY and WL performed optical calculation and wrote part of first draft. PT and MD provided the online measurement data of new particle formation and growth. JS and XZ coordinated the field campaign. All authors commented and edited the paper.

Competing interests: The authors declare no competing financial interests

Acknowledgments We thank Boris Quennehen to provide data from the FLEXPART-WRF. This work was funded by National Natural Science Foundation of China (41622504, 41575116, 31700475) and the Hundred Talents Program in Zhejiang University, Z.S. acknowledges funding from NERC (NE/S00579X/1).

References

Abbatt, J.P.D., Leaitch, W.R., Aliabadi, A.A., Bertram, A.K., Blanchet, J.P., Boivin-Rioux, A., Bozem, H., Burkart, J., Chang, R.Y.W., Charette, J., Chaubey, J.P., Christensen, R.J., Cirisan, A., Collins, D.B., Croft, B., Dionne, J., Evans, G.J., Fletcher, C.G., Galí, M., Ghahremaninezhad, R., Girard, E., Gong, W., Gosselin, M., Gourdal, M., Hanna, S.J., Hayashida, H., Herber, A.B., Hesaraki, S., Hoor, P., Huang, L., Hussherr, R., Irish, V.E., Keita, S.A., Kodros, J.K., Köllner, F., Kolonjari, F., Kunkel, D., Ladino, L.A., Law, K., Levasseur, M., Libois, Q., Liggio, J., Lizotte, M., Macdonald, K.M., Mahmood, R., Martin, R.V., Mason, R.H., Miller, L.A., Moravek, A., Mortenson, E., Mungall, E.L., Murphy, J.G., Namazi, M., Norman, A.L., O'Neill, N.T., Pierce, J.R., Russell, L.M., Schneider, J., Schulz, H., Sharma, S., Si, M., Staebler, R.M., Steiner, N.S., Thomas, J.L., von Salzen, K., Wentzell, J.J.B., Willis, M.D., Wentworth, G.R., Xu, J.W., Yakobi-Hancock, J.D.: Overview paper: New insights into aerosol and climate in the Arctic, Atmos. Chem. Phys., 19 (4), 2527-2560, 2019.

Alexander, D.T.L., Crozier, P.A., Anderson, J.R.: Brown Carbon Spheres in East Asian Outflow and Their Optical Properties, Science, 321 (5890), 833-836, 2008.

Andreae, M.O., Gelencser, A.: Black carbon or brown carbon? The nature of light-absorbing carbonaceous aerosols, Atmos. Chem. Phys., 6 (10), 3131-3148, 2006.

Behrenfeldt, U., Krejci, R., Ström, J., Stohl, A.: Chemical properties of Arctic aerosol particles collected at the Zeppelin station during the aerosol transition period in May and June of 2004, Tellus B, 60 (3), 405-415, 2008.

Bohren, C.F., Huffman, D.R., 1983. Absorption and scattering of light by small particles. John Wiley & Sons, Inc. , New York, USA.

Bond, T.C., Doherty, S.J., Fahey, D.W., Forster, P.M., Berntsen, T., DeAngelo, B.J., Flanner, M.G., Ghan, S., Kärcher, B., Koch, D., Kinne, S., Kondo, Y., Quinn, P.K., Sarofim, M.C., Schultz, M.G., Schulz, M., Venkataraman, C., Zhang, H., Zhang, S., Bellouin, N., Guttikunda, S.K., Hopke, P.K., Jacobson, M.Z., Kaiser, J.W., Klimont, Z., Lohmann, U., Schwarz, J.P., Shindell, D., Storelvmo, T., Warren, S.G., Zender, C.S.: Bounding the role of black carbon in the climate system: A scientific assessment, J. Geophys. Res., 118 (11), 5380-5552, 2013.

Brioude, J., Arnold, D., Stohl, A., Cassiani, M., Morton, D., Seibert, P., Angevine, W., Evan, S., Dingwell, A., Fast, J.D., Easter, R.C., Pisso, I., Burkhart, J., Wotawa, G.: The Lagrangian particle dispersion model FLEXPART-WRF version 3.1, Geosci. Model Dev., 6 (6), 1889-1904, 2013.

Brock, C.A., Cozic, J., Bahreini, R., Froyd, K.D., Middlebrook, A.M., McComiskey, A., Brioude, J., Cooper, O.R., Stohl, A., Aikin, K.C., de Gouw, J.A., Fahey, D.W., Ferrare, R.A., Gao, R.S., Gore, W., Holloway, J.S., Hübler, G., Jefferson, A., Lack, D.A., Lance, S., Moore, R.H., Murphy, D.M., Nenes, A., Novelli, P.C., Nowak, J.B., Ogren, J.A., Peischl, J., Pierce, R.B., Pilewskie, P., Quinn, P.K., Ryerson, T.B., Schmidt, K.S., Schwarz, J.P., Sodemann, H., Spackman, J.R., Stark, H., Thomson, D.S., Thornberry, T., Veres, P., Watts, L.A., Warneke, C., Wollny, A.G.: Characteristics, sources, and transport of aerosols measured in spring 2008 during the aerosol, radiation, and cloud processes affecting Arctic Climate (ARCPAC) Project, Atmos. Chem. Phys., 11 (6), 2423-2453, 2011.

Browse, J., Carslaw, K.S., Schmidt, A., Corbett, J.J.: Impact of future Arctic shipping on high-latitude black carbon deposition, Geophys. Res. Lett.,, 40 (16), 4459-4463, 2013.

Burkart, J., Willis, M.D., Bozem, H., Thomas, J.L., Law, K., Hoor, P., Aliabadi, A.A., Köllner, F., Schneider, J., Herber, A., Abbatt, J.P.D., Leaitch, W.R.: Summertime observations of elevated levels of ultrafine particles in the high Arctic marine boundary layer, Atmos. Chem. Phys., 17 (8),

5515-5535, 2017.

Buseck, P.R., Posfai, M.: Airborne minerals and related aerosol particles: Effects on climate and the environment, P. Natl. Acad. Sci. USA, 96 (7), 3372-3379, 1999.

Chang, R.Y.W., Leck, C., Graus, M., Müller, M., Paatero, J., Burkhart, J.F., Stohl, A., Orr, L.H., Hayden, K., Li, S.M., Hansel, A., Tjernström, M., Leaitch, W.R., Abbatt, J.P.D.: Aerosol composition and sources in the central Arctic Ocean during ASCOS, Atmos. Chem. Phys., 11 (20), 10619-10636, 2011.

Chi, J.W., Li, W.J., Zhang, D.Z., Zhang, J.C., Lin, Y.T., Shen, X.J., Sun, J.Y., Chen, J.M., Zhang, X.Y., Zhang, Y.M., Wang, W.X.: Sea salt aerosols as a reactive surface for inorganic and organic acidic gases in the Arctic troposphere, Atmos. Chem. Phys., 15 (19), 11341-11353, 2015.

Dagsson-Waldhauserova, P., Arnalds, O., Olafsson, H.: Long-term frequency and characteristics of dust storm events in Northeast Iceland (1949–2011), Atmos. Environ., 77 (0), 117-127, 2013.

Dall'Osto, M., Beddows, D.C.S., Tunved, P., Krejci, R., Ström, J., Hansson, H.C., Yoon, Y.J., Park, K.-T., Becagli, S., Udisti, R., Onasch, T., O'Dowd, C.D., Simó, R., Harrison, R.M.: Arctic sea ice melt leads to atmospheric new particle formation, Sci. Rep., 7 (1), 3318, 2017.

Doherty, S.J., Grenfell, T.C., Forsström, S., Hegg, D.L., Brandt, R.E., Warren, S.G.: Observed vertical redistribution of black carbon and other insoluble light-absorbing particles in melting snow, J. Geophys. Res., 118 (11), 5553-5569, 2013.

Feng, Y., Ramanathan, V., Kotamarthi, V.R.: Brown carbon: a significant atmospheric absorber of solar radiation?, Atmos. Chem. Phys., 13 (17), 8607-8621, 2013.

Fu, P., Kawamura, K., Barrie, L.A.: Photochemical and Other Sources of Organic Compounds in the Canadian High Arctic Aerosol Pollution during Winter−Spring, Environ. Sci. Technol., 43 (2), 286-292, 2008.

Geng, H., Ryu, J., Jung, H.-J., Chung, H., Ahn, K.-H., Ro, C.-U.: Single-Particle Characterization of Summertime Arctic Aerosols Collected at Ny-Alesund, Svalbard, Environ. Sci. Technol., 44 (7), 2348-2353, 2010.

Ghosal, S., Weber, P.K., Laskin, A.: Spatially resolved chemical imaging of individual atmospheric particles using nanoscale imaging mass spectrometry: insight into particle origin and chemistry, Analytical Methods, 6 (8), 2444-2451, 2014.

Gilgen, A., Huang, W.T.K., Ickes, L., Neubauer, D., Lohmann, U.: How important are future marine and shipping aerosol emissions in a warming Arctic summer and autumn?, Atmos. Chem. Phys., 18 (14), 10521-10555, 2018.

Hansen, J., Nazarenko, L.: Soot climate forcing via snow and ice albedos, P. Natl. Acad. Sci. USA, 101 (2), 423-428, 2004.

Hara, K., Yamagata, S., Yamanouchi, T., Sato, K., Herber, A., Iwasaka, Y., Nagatani, M., Nakata, H.: Mixing states of individual aerosol particles in spring Arctic troposphere during ASTAR 2000 campaign, J. Geophys. Res., 108 (D7), 2003.

Hegg, D.A., Warren, S.G., Grenfell, T.C., Sarah, J.D., Clarke, A.D.: Sources of light-absorbing aerosol in arctic snow and their seasonal variation, Atmos. Chem. Phys., 10 (22), 10923-10938, 2010.

Herrmann, A.M., Ritz, K., Nunan, N., Clode, P.L., Pett-Ridge, J., Kilburn, M.R., Murphy, D.V., O'Donnell, A.G., Stockdale, E.A.: Nano-scale secondary ion mass spectrometry — A new analytical tool in biogeochemistry and soil ecology: A review article, Soil Biol. Biochem., 39 (8), 1835-1850, 2007.

IPCC (2013), Clouds and Aerosols, in Climate Change 2013: The Physical Science Basis. Contribution

of Working Group I to the Fifth Assessment Report of the Intergovernmental Panel on Climate Change, 571-657 pp, Cambridge, U.K. and New York, NY.

Iwasaka, Y., Minoura, H., Nagaya, K.: The transport and spatial scale of Asian dust-storm clouds: A case study of the dust-storm event of April 1979, Tellus, Ser. B, 35, 189-196, 1983.

Iziomon, M.G., Lohmann, U., Quinn, P.K.: Summertime pollution events in the Arctic and potential implications, J. Geophys. Res., 111 (D12), D12206, 2006.

Jacob, D.J., Crawford, J.H., Maring, H., Clarke, A.D., Dibb, J.E., Emmons, L.K., Ferrare, R.A., Hostetler, C.A., Russell, P.B., Singh, H.B., Thompson, A.M., Shaw, G.E., McCauley, E., Pederson, J.R., Fisher, J.A.: The Arctic Research of the Composition of the Troposphere from Aircraft and Satellites (ARCTAS) mission: design, execution, and first results, Atmos. Chem. Phys., 10 (11), 5191-5212, 2010.

Jiang, H., Frie, A.L., Lavi, A., Chen, J.Y., Zhang, H., Bahreini, R., Lin, Y.-H.: Brown Carbon Formation from Nighttime Chemistry of Unsaturated Heterocyclic Volatile Organic Compounds, Environ. Sci. Techn. Lett., DOI: 10.1021/acs.estlett.1029b00017, 2019.

Karl, M., Leck, C., Coz, E., Heintzenberg, J.: Marine nanogels as a source of atmospheric nanoparticles in the high Arctic, Geophys. Res. Lett.,, 40 (14), 3738-3743, 2013.

Kirpes, R.M., Bondy, A.L., Bonanno, D., Moffet, R.C., Wang, B., Laskin, A., Ault, A.P., Pratt, K.A.: Secondary sulfate is internally mixed with sea spray aerosol and organic aerosol in the winter Arctic, Atmos. Chem. Phys., 18 (6), 3937-3949, 2018.

Koch, D., Hansen, J.: Distant origins of Arctic black carbon: A Goddard Institute for Space Studies ModelE experiment, J. Geophys. Res., 110 (D4), D04204, 2005.

Lack, D.A., Langridge, J.M., Bahreini, R., Cappa, C.D., Middlebrook, A.M., Schwarz, J.P.: Brown carbon and internal mixing in biomass burning particles, P. Natl. Acad. Sci. USA, 109 (37), 14802-14807, 2012.

Laskin, A., Laskin, J., Nizkorodov, S.A.: Chemistry of Atmospheric Brown Carbon, Chem. Rev., 115 (10), 4355-4382, 2015.

Laskina, O., Morris, H.S., Grandquist, J.R., Estillore, A.D., Stone, E.A., Grassian, V.H., Tivanski, A.V.: Substrate-Deposited Sea Spray Aerosol Particles: Influence of Analytical Method, Substrate, and Storage Conditions on Particle Size, Phase, and Morphology, Environ. Sci. Tech., 49 (22), 13447-13453, 2015.

Lathem, T.L., Beyersdorf, A.J., Thornhill, K.L., Winstead, E.L., Cubison, M.J., Hecobian, A., Jimenez, J.L., Weber, R.J., Anderson, B.E., Nenes, A.: Analysis of CCN activity of Arctic aerosol and Canadian biomass burning during summer 2008, Atmos. Chem. Phys., 13 (5), 2735-2756, 2013.

Law, K.S., Stohl, A.: Arctic Air Pollution: Origins and Impacts, Science, 315 (5818), 1537-1540, 2007.

Leck, C., Bigg, E.K.: Comparison of sources and nature of the tropical aerosol with the summer high Arctic aerosol, Tellus, Ser. B, 60 (1), 118-126, 2008.

Leck, C., Svensson, E.: Importance of aerosol composition and mixing state for cloud droplet activation over the Arctic pack ice in summer, Atmos. Chem. Phys., 15 (5), 2545-2568, 2015.

Li, W., Sun, J., Xu, L., Shi, Z., Riemer, N., Sun, Y., Fu, P., Zhang, J., Lin, Y., Wang, X., Shao, L., Chen, J., Zhang, X., Wang, Z., Wang, W.: A conceptual framework for mixing structures in individual aerosol particles, J. Geophys. Res., 121 (22), 13,784-713,798, 2016.

Li, W., Xu, L., Liu, X., Zhang, J., Lin, Y., Yao, X., Gao, H., Zhang, D., Chen, J., Wang, W., Harrison, R.M., Zhang, X., Shao, L., Fu, P., Nenes, A., Shi, Z.: Air pollution–aerosol interactions produce more bioavailable iron for ocean ecosystems, Sci. Adv., 3 (3), e1601749, 2017.

Maahn, M., de Boer, G., Creamean, J.M., Feingold, G., McFarquhar, G.M., Wu, W., Mei, F.: The observed influence of local anthropogenic pollution on northern Alaskan cloud properties, Atmos. Chem. Phys., 17 (23), 14709-14726, 2017.

Martin, M., Chang, R.Y.W., Sierau, B., Sjogren, S., Swietlicki, E., Abbatt, J.P.D., Leck, C., Lohmann, U.: Cloud condensation nuclei closure study on summer arctic aerosol, Atmos. Chem. Phys., 11 (22), 11335-11350, 2011.

Moffet, R.C., Rödel, T.C., Kelly, S.T., Yu, X.Y., Carroll, G.T., Fast, J., Zaveri, R.A., Laskin, A., Gilles, M.K.: Spectro-microscopic measurements of carbonaceous aerosol aging in Central California, Atmos. Chem. Phys., 13 (20), 10445-10459, 2013.

Moore, R.H., Bahreini, R., Brock, C.A., Froyd, K.D., Cozic, J., Holloway, J.S., Middlebrook, A.M., Murphy, D.M., Nenes, A.: Hygroscopicity and composition of Alaskan Arctic CCN during April 2008, Atmos. Chem. Phys., 11 (22), 11807-11825, 2011.

Moroni, B., Cappelletti, D., Crocchianti, S., Becagli, S., Caiazzo, L., Traversi, R., Udisti, R., Mazzola, M., Markowicz, K., Ritter, C., Zielinski, T.: Morphochemical characteristics and mixing state of long range transported wildfire particles at Ny-Ålesund (Svalbard Islands), Atmos. Environ., 156, 135-145, 2017.

Park, K., Kim, G., Kim, J.-s., Yoon, Y.-J., Cho, H.-j., Ström, J.: Mixing State of Size-Selected Submicrometer Particles in the Arctic in May and September 2012, Environ. Sci. Technol., 48 (2), 909-919, 2013.

Peters, G.P., Nilssen, T.B., Lindholt, L., Eide, M.S., Glomsrød, S., Eide, L.I., Fuglestvedt, J.S.: Future emissions from shipping and petroleum activities in the Arctic, Atmos. Chem. Phys., 11 (11), 5305-5320, 2011.

Qi, L., Li, Q., Li, Y., He, C.: Factors controlling black carbon distribution in the Arctic, Atmos. Chem. Phys., 17 (2), 1037-1059, 2017.

Quinn, P.K., Shaw, G., Andrews, E., Dutton, E.G., Ruoho-Airola, T., Gong, S.L.: Arctic haze: current trends and knowledge gaps, Tellus B, 59 (1), 99-114, 2007.

Raatikainen, T., Brus, D., Hyvärinen, A.P., Svensson, J., Asmi, E., Lihavainen, H.: Black carbon concentrations and mixing state in the Finnish Arctic, Atmos. Chem. Phys., 15 (17), 10057-10070, 2015.

Riemer, N., West, M., Zaveri, R.A., Easter, R.C.: Simulating the evolution of soot mixing state with a particle resolved aerosol model, J. Geophys. Res., 114, doi:10.1029/2008JD011073, 2009.

Saleh, R., Hennigan, C.J., McMeeking, G.R., Chuang, W.K., Robinson, E.S., Coe, H., Donahue, N.M., Robinson, A.L.: Absorptivity of brown carbon in fresh and photo-chemically aged biomass-burning emissions, Atmos. Chem. Phys., 13 (15), 7683-7693, 2013.

Samset, B.H., Myhre, G., Herber, A., Kondo, Y., Li, S.M., Moteki, N., Koike, M., Oshima, N., Schwarz, J.P., Balkanski, Y., Bauer, S.E., Bellouin, N., Berntsen, T.K., Bian, H., Chin, M., Diehl, T., Easter, R.C., Ghan, S.J., Iversen, T., Kirkevåg, A., Lamarque, J.F., Lin, G., Liu, X., Penner, J.E., Schulz, M., Seland, Ø., Skeie, R.B., Stier, P., Takemura, T., Tsigaridis, K., Zhang, K.: Modelled black carbon radiative forcing and atmospheric lifetime in AeroCom Phase II constrained by aircraft observations, Atmos. Chem. Phys., 14 (22), 12465-12477, 2014.

Sand, M., Berntsen, T.K., Kay, J.E., Lamarque, J.F., Seland, Ø., Kirkevåg, A.: The Arctic response to remote and local forcing of black carbon, Atmos. Chem. Phys., 13 (1), 211-224, 2013.

Seinfeld, J., Pandis, S., 2006. Atmospheric Chemistry and Physics: From air pollution to climate change (2nd ed.). 1-1203 pp., John Wiley & Son, Inc., Hoboken, New Jersey.

Shindell, D.: Local and remote contributions to Arctic warming, Geophys. Res. Lett.,, 34 (14), L14704, 2007.

Sierau, B., Chang, R.Y.W., Leck, C., Paatero, J., Lohmann, U.: Single-particle characterization of the high-Arctic summertime aerosol, Atmos. Chem. Phys., 14 (14), 7409-7430, 2014.

Updyke, K.M., Nguyen, T.B., Nizkorodov, S.A.: Formation of brown carbon via reactions of ammonia with secondary organic aerosols from biogenic and anthropogenic precursors, Atmos. Environ., 63 (0), 22-31, 2012.

Wöhrnschimmel, H., MacLeod, M., Hungerbuhler, K.: Emissions, Fate and Transport of Persistent Organic Pollutants to the Arctic in a Changing Global Climate, Environ. Sci. Technol., 47 (5), 2323-2330, 2013.

Wang, B., Laskin, A., Roedel, T., Gilles, M.K., Moffet, R.C., Tivanski, A.V., Knopf, D.A.: Heterogeneous ice nucleation and water uptake by field-collected atmospheric particles below 273 K, J. Geophys. Res., 117, 2012.

Wang, X., Heald, C.L., Liu, J., Weber, R.J., Campuzano-Jost, P., Jimenez, J.L., Schwarz, J.P., Perring, A.E.: Exploring the observational constraints on the simulation of brown carbon, Atmos. Chem. Phys., 18 (2), 635-653, 2018.

Weinbruch, S., Wiesemann, D., Ebert, M., Schütze, K., Kallenborn, R., Ström, J.: Chemical composition and sources of aerosol particles at Zeppelin Mountain (Ny Ålesund, Svalbard): An electron microscopy study, Atmos. Environ., 49 (0), 142-150, 2012.

Winiger, P., Andersson, A., Eckhardt, S., Stohl, A., Gustafsson, Ö.: The sources of atmospheric black carbon at a European gateway to the Arctic, Nat. Commun., 7, 12776, 2016.

Winiger, P., Andersson, A., Eckhardt, S., Stohl, A., Semiletov, I.P., Dudarev, O.V., Charkin, A., Shakhova, N., Klimont, Z., Heyes, C., Gustafsson, Ö.: Siberian Arctic black carbon sources constrained by model and observation, P. Natl. Acad. Sci. USA, 114 (7), E1054-E1061, 2017.

Xu, J.W., Martin, R.V., Morrow, A., Sharma, S., Huang, L., Leaitch, W.R., Burkart, J., Schulz, H., Zanatta, M., Willis, M.D., Henze, D.K., Lee, C.J., Herber, A.B., Abbatt, J.P.D.: Source attribution of Arctic black carbon constrained by aircraft and surface measurements, Atmos. Chem. Phys., 17 (19), 11971-11989, 2017.

Yang, Y., Wang, H., Smith, S.J., Easter, R.C., Rasch, P.J.: Sulfate Aerosol in the Arctic: Source Attribution and Radiative Forcing, J. Geophys. Res., 123 (3), 1899-1918, 2018.

You, Y., Renbaum-Wolff, L., Carreras-Sospedra, M., Hanna, S.J., Hiranuma, N., Kamal, S., Smith, M.L., Zhang, X., Weber, R.J., Shilling, J.E., Dabdub, D., Martin, S.T., Bertram, A.K.: Images reveal that atmospheric particles can undergo liquid–liquid phase separations, P. Natl. Acad. Sci. USA, 109 (33), 13188-13193, 2012.

Zanatta, M., Laj, P., Gysel, M., Baltensperger, U., Vratolis, S., Eleftheriadis, K., Kondo, Y., Dubuisson, P., Winiarek, V., Kazadzis, S., Tunved, P., Jacobi, H.W.: Effects of mixing state on optical and radiative properties of black carbon in the European Arctic, Atmos. Chem. Phys., 18 (19), 14037-14057, 2018.

Zangrando, R., Barbaro, E., Zennaro, P., Rossi, S., Kehrwald, N.M., Gabrieli, J., Barbante, C., Gambaro, A.: Molecular Markers of Biomass Burning in Arctic Aerosols, Environ. Sci. Technol., 47 (15), 8565-8574, 2013.

Figure Captions

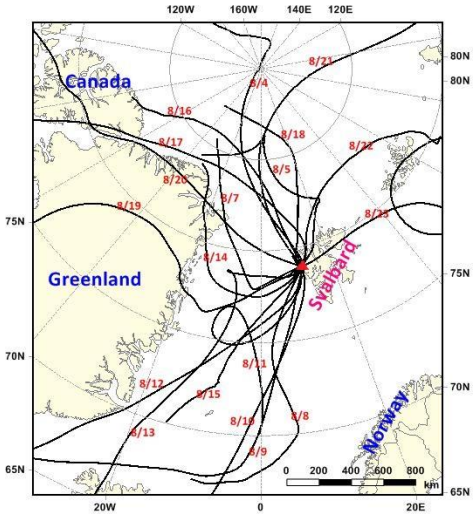

Figure 1 72 h back trajectories of air masses at 500m over Arctic Yellow River Station in Svalbard during 3–26 August 2012, and arriving time was set according to the sampling time

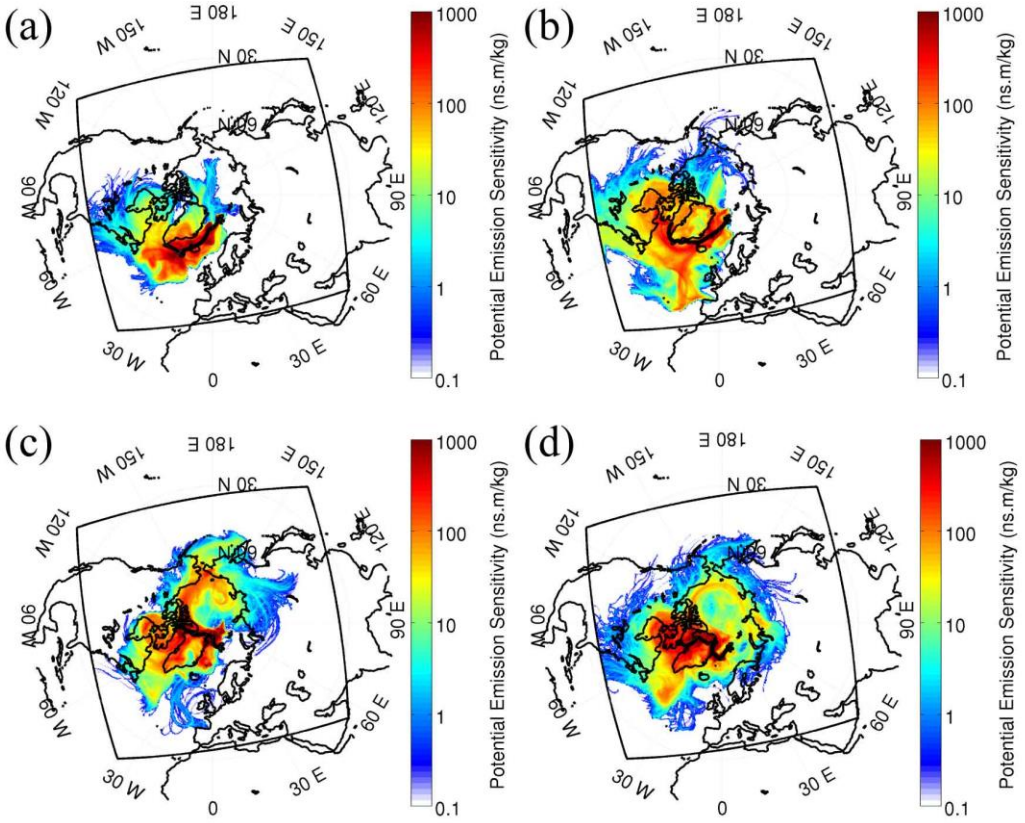

Figure 2 FLEXPART-WRF PES on August 11, 12, 14, and 15, 2012. Black square is showing the WRF domain used to initiate the FLEXPART-WRF simulation.

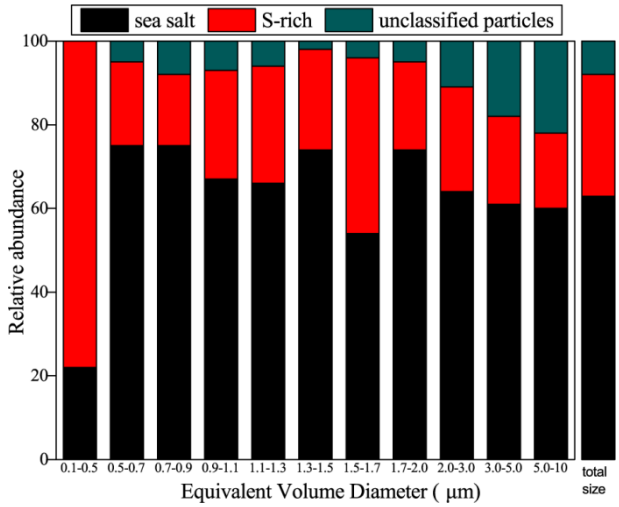

Figure 3 Morphology and relative abundances of typical individual aerosol particles in the 21 analyzed samples.

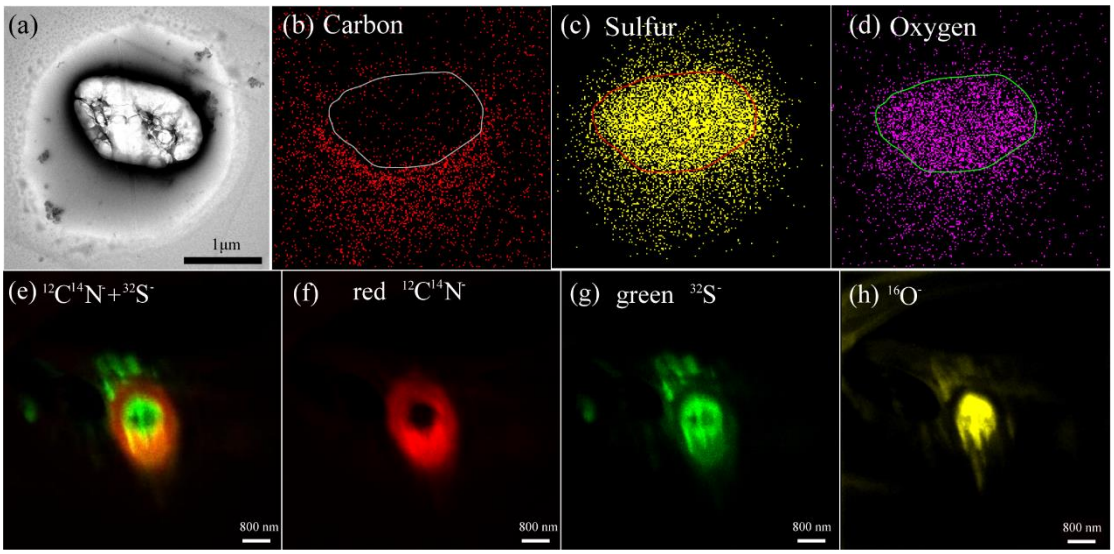

Figure 4 TEM Observations of a secondary particle and NanoSIMS intensity threshold maps of an aerosol particle with sulfate core and OM coating. (a) Bright-field TEM image of an internally mixed particle; (b) elemental carbon (c) sulfur and (d) oxygen maps of the internally mixed particle shown in 1(a); (e) Overlay of $^{12}C^{14}N^{-}$ and $^{32}S^{-}$ ion maps in an internally mixed particle; (f) CN^{-} map (g) S^{-} (h) O^{-} secondary ion maps. Ion maps with a set of aerosol particles were shown in Figure S1.

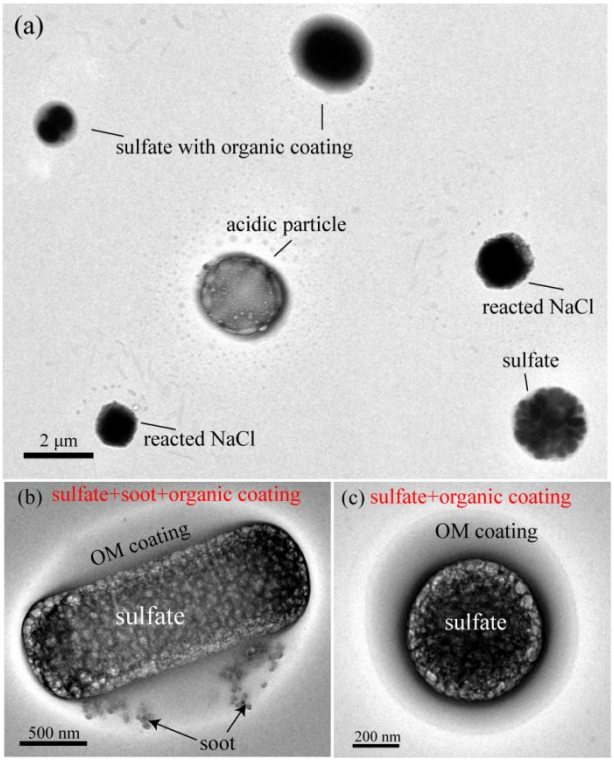

Figure 5 TEM images of individual particles containing sulfate, OM, and soot. (a) Low magnification TEM image showing sulfates, sulfate with OM coating, and reacted NaCl particles. (b) an internally mixed particle of sulfate and soot with OM coating (c) a particle with sulfate core and OM coating.

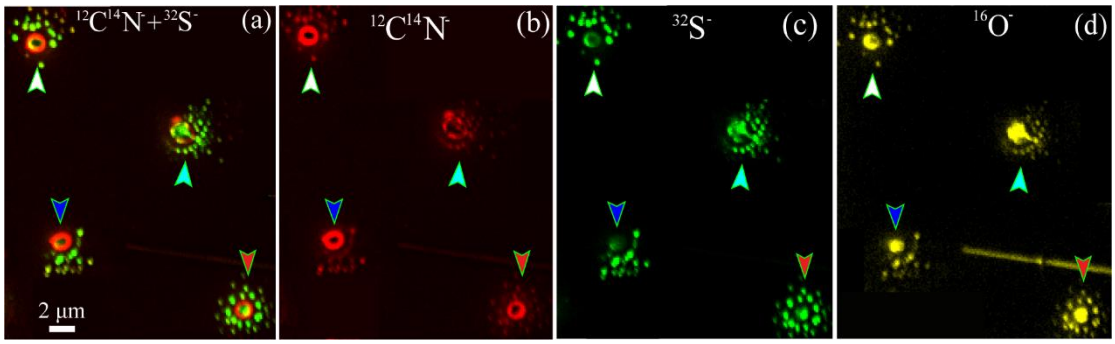

Figure 6 NanoSIMS intensity threshold maps of individual aerosol particles surrounded by satellite particles. (e) Overlay of $^{12}C^{14}N^{-}$and $^{32}S^{-}$ ion maps of individual particles. (f) CN^{-} (g) S^{-} (h) O^{-} maps. Four particles were indicated by white, pink, blue, and red arrows.

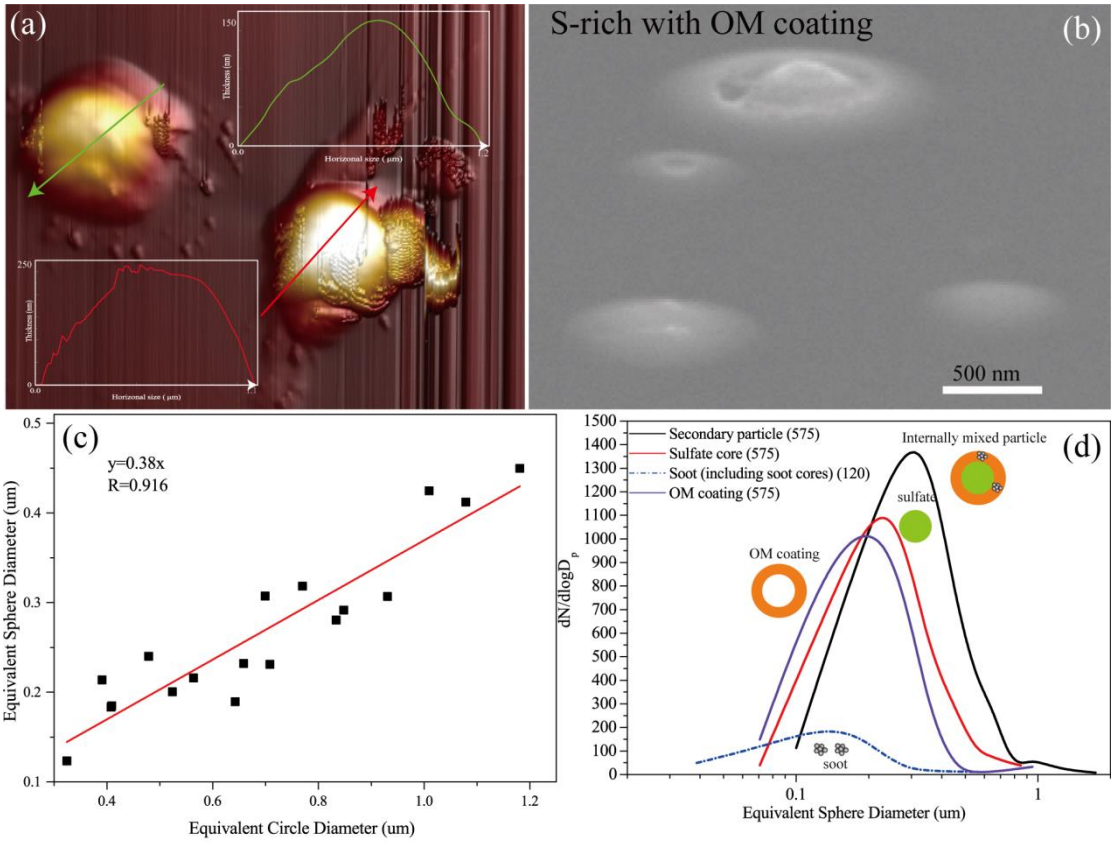

Figure 7 Secondary particles on the substrate. (a) 3-D AFM image of secondary sulfate particles. The colorful arrows represent particles surface properites of the particle section. (b) SEM image of S-rich with OM coating obtained from 75^{o} tilt of the SEM specimen stage (c) The near linear relationships between ECD and ESD based on S-rich particles with thick OM coating by Atomic force microscopy. (d) Size distribution of individual particle with OM coating and sulfate cores based on the estimated ESD diameter from TEM image. Sizes of soot particles are equal to the equivalent circle diameter.

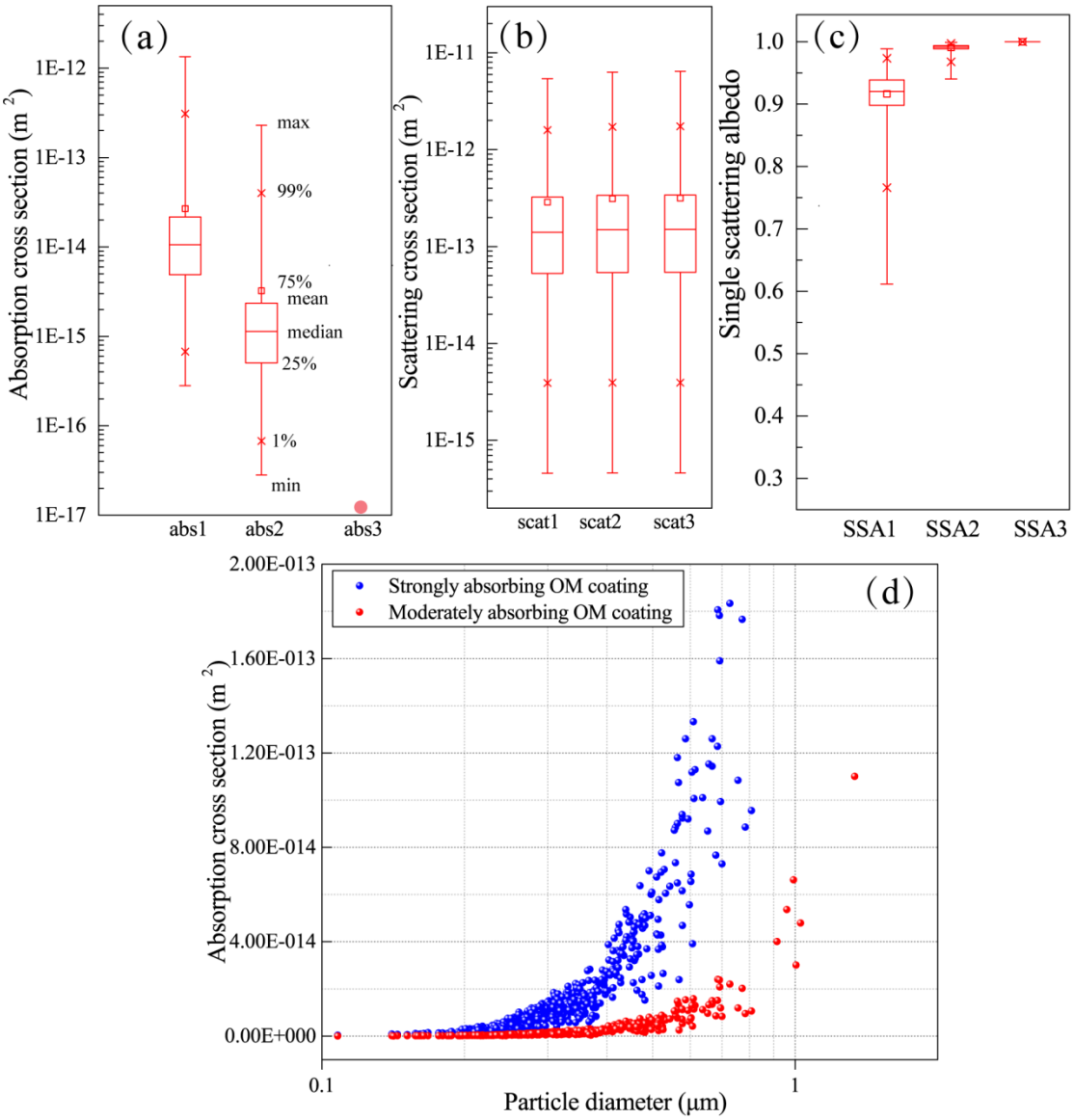

Figure 8 Optical properties of Box-and-whisker plots showing optical parameters of all analysed particles assuming sulfate core and BrC shell (not considering soot cores in the particles). (a) Scattering cross section (b) Absorption cross section (c) Single scattering albedo. Top to bottom makers in the box-and-whisker represent max, 99%, 75%, mean, median, 25%, 1%, min values. (d) Absorption cross section along with particle diameter assuming strongly absorbing BrC and Moderate absorbing BrC as the particle OM coating.